Macromolecules
ARTICLE

Macromolecules **2010**, *43*, 6903–6911 **6903**
DOI: 10.1021/ma101138w

Brownian Dynamics Simulations on Self-Assembly Behavior of H-Shaped Copolymers and Terpolymers.

Othonas Moultos, Leonidas N. Gergidis, and Costas Vlahos*

Department of Chemistry, University of Ioannina, 45110 Ioannina, Greece

Received May 21, 2010; Revised Manuscript Received July 10, 2010

ABSTRACT: The micellization behavior of the H-shaped copolymers and terpolymers is studied by means of Brownian dynamics simulations. The critical micelle concentration, the micelle size distribution and the shape of micelles are examined as a function of the mass fraction of the solvophobic units. Three regimes were found. H-shaped copolymers with solvophobic content $\geq 50\%$ form micelles with preferential aggregation number. Those with content $\ll 10\%$ do not aggregate at the simulation temperature. For the remaining content values the formation of micelles exhibits a wide variation of aggregation numbers. These regimes are in qualitative agreement with the experimental findings. H-shaped terpolymers form micelles with larger aggregation number than the respective H-shaped copolymers. Janus-like micelles or micelles with multicompartment coronas are obtained.

1. Introduction

Linear AB diblock copolymers dissolved in selective solvent present similarities with surfactants and self-assemble into mesoscopic objects. Beyond a particular polymer concentration, which is known as the critical micelle concentration (cmc), the polymeric surfactants form the so-called micelles. A micelle consists of a dense solvophobic core and an extended solvophilic corona. The intrinsic advantage of diblock copolymers over the low molecular weight surfactants is that the length of each block can be widely varied without losing the thermodynamic stability of the micelles. Thus, amphiphilic diblock copolymers are used in various applications such as detergency, dispersion stabilization, lubrication, and drug carriers of hydrophobic drugs.[1]

The micelallization properties of linear diblock copolymers in selective solvents have attracted the attention of many research groups in the past few decades.[2] It was found that they form almost monochromatic micelles with increasing aggregation number when the ratio of solvophobic to solvophilic units and the total molecular weight of the copolymer are both increased. The thickness of the dense core and of the extended corona are influenced by the same parameters (molecular weight, solvophobic to solvophilic ratio), allowing flexibility in adjusting the copolymers for a particular application. The structural characteristics of the micelles are influenced by a variety of factors, such as the chemical nature of A and B blocks, temperature, concentration, and the architecture of the copolymer.[2]

Because of the progress in polymer synthesis, model copolymers with complex architecture as miktoarm star,[3] starblock,[4] dentritic,[5] graft,[6] H-shaped,[7] super H-shaped,[8] and π-shaped[7] are available, and their studies[2−12] facilitate the further understanding of polymer structure-micelle relations. Indeed, experimental work on super H-shaped block copolymers,[8] consisting of a polystyrene (PS) central block and two polyisoprene (PI) three arm stars each connected to PS end groups, in *n*-decane solvent, demonstrate a completely different micellalization behavior compared to the respective linear copolymers with the same molecular weights. Normal (*n*-) decane is a nonsolvent for PS and a good solvent for PI. Super H-shaped copolymers with a small weight fraction (14%) of PS do not aggregate under a variety of experimental conditions. Those with increased weight fraction ($>33\%$) of PS are formed into monodisperse spherical micelles, with aggregation number considerably lower than those formed by linear PS/PI block copolymers. For intermediate PS weight fractions ($>14\%$ and $<33\%$) super H-shaped copolymers form micelles with a variety of aggregation numbers.

In general, architectures similar to those of super H-shaped copolymers, where solvophilic moieties with star, dendritic or other architecture are connected at both ends of the solvophobic bridge, can lead to the formation of Janus molecules or micelles.[9] The necessary condition for obtaining Janus molecules or micelles is the existence of strong chemical mismatch between the two solvophilic moieties connected to the different bridge ends. Janus H-shaped terpolymers with incompatible PS and polydimethylsiloxane (PDMS) branches and polybutadiene (PBd) bridge have been synthesized.[9] The micellar behavior was studied[9] by static and dynamic light scattering in methyl ethyl ketone (MEK), a selective solvent for PS and PDMS blocks. The samples with relatively short PBd bridge formed unimolecular micelles, while a sample with longer bridge formed micelles with a very low aggregation number (equal to 2). The intrinsic asymmetry of the Janus particles (JP) having different atomic-molecular quantities and properties (such as charge, polarity and optical and magnetic) at opposite sides make them unique among other nanoparticles. Recently the JP demonstrated huge potential as drug carriers, emulsion stabilizers, and functional elements for design of electronic paper.[13]

Despite the aforementioned potential in applications the complexity of H-shaped copolymer and terpolymer architecture has restricted the theoretical and experimental studies reported in the literature. We employed Brownian dynamics simulations[14] in order to elucidate the effects of the H-shaped architecture on the micellalization behavior. Brownian dynamics has successfully been used in the study of other complex architectures, such as dendritic[11] and graft[12] copolymers, for the investigation of self-assembly of rod−coil copolymers[15] and peptides.[16] It is expected that Brownian dynamics to be also appropriate for the study of

*Corresponding author. E-mail: cvlahos@cc.uoi.gr.

Published on Web 07/26/2010

H-shaped copolymers and terpolymers. The properties of interest are the critical micelle concentration, the mean aggregation number, and the shape of the micelle which is expressed by the asphericity, the acylindricity, the thickness of the corona, and the solvophobic core radius. In addition, we report direct comparisons of our simulation results with experimental[8,9] findings and simulation studies of similar systems[11] existing in the literature.

2. Model

We employed a coarse-grained model to represent the amphiphilic copolymers and terpolymers. As we aimed at a qualitative description of the effects of the H-shaped architecture on the self-assembly, we assume that this model is adequate. A group of atoms were modeled as a bead (with diameter σ), while different beads were connected with flexible finite extended elastic bonds (FENE). The FENE potential is expressed as

$$U_{Bond}(r_{ij}) = \begin{cases} -0.5kR_0^2 \ln\left[1-\left(\frac{r_{ij}}{R_0}\right)^2\right], & r_{ij} \le R_0 \\ \infty, & r_{ij} > R_0 \end{cases} \quad (1)$$

where r_{ij} is the distance between beads i and j, $k = 25T\varepsilon/\sigma^2$ and R_0 is the maximum extent of the bond ($R_0 = 1.5\sigma$). These parameters[11,26] prevent chain crossing by ensuring an average bond length of 0.97σ. Monomer−monomer interactions were calculated by means of a truncated and shifted Lennard-Jones potential:

$$U_{LJ}(r_{ij}) = \begin{cases} 4\varepsilon_{ij}\left[\left(\frac{\sigma}{r_{ij}}\right)^{12} - \left(\frac{\sigma}{r_{ij}}\right)^{6} - \left(\frac{\sigma}{r_{cij}}\right)^{12} + \left(\frac{\sigma}{r_{cij}}\right)^{6}\right] + \varepsilon_{ij}, & r_{ij} \le r_{cij} \\ 0, & r_{ij} > r_{cij} \end{cases} \quad (2)$$

where ε_{ij} is the well-depth, and r_{cij} is the cutoff radius. The solvent molecules are considered implicitly. The short timesteps needed to model the solvent behavior (the fast motion) restrict the time scales that maybe sampled, thereby limiting the information that can be obtained for the slower motion of the copolymer. Brownian dynamics simulation method allows the statistical treatment of the solvent, incorporating its influence on the copolymer by a combination of random forces and frictional terms. The friction coefficient and the random force couple the simulated system to a heat bath and therefore the simulation has canonical ensemble (NVT) constraints. The equation of motion of each bead i of mass m in the simulation box follows the Langevin equation:

$$m_i\ddot{\mathbf{r}}_i(t) = -\nabla\sum_j[U_{LJ}(r_{ij}) + U_{Bond}(r_{ij})] - m_i\xi\dot{\mathbf{r}}_i(t) + \boldsymbol{F}_i(t) \quad (3)$$

where m_i, $\boldsymbol{r}_i$, and ξ are the mass, the position vector, and the friction coefficient of the i bead, respectively. The friction coefficient is equal to $\xi = 0.5\tau^{-1}$, with

$$\tau = \sigma\sqrt{m/\varepsilon}$$

The random force vector $\boldsymbol{F}_i$ is assumed to be Gaussian, with zero mean, and satisfies the equation

$$\langle \mathbf{F}_i(t)\cdot\mathbf{F}_j(t')\rangle = 6k_{\mathrm{B}}Tm\xi\delta_{ij}\delta(t-t') \quad (4)$$

k_B is the Boltzmann constant, and T is the temperature.

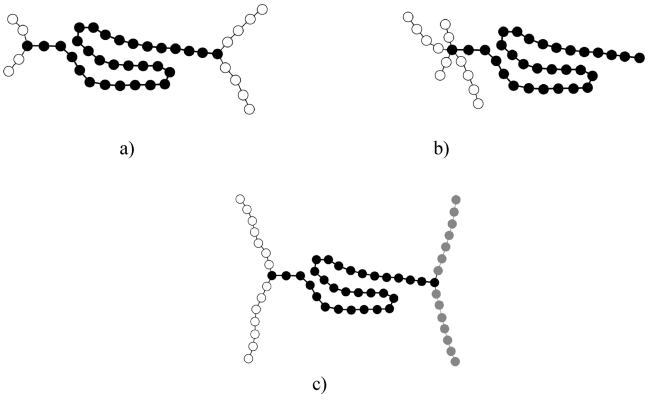

Figure 1. Cartoon representation of (a) H-shaped copolymer $(A_2)_2$-$B_{30}(A_4)_2$, (b) miktoarm star copolymer $(A_2)_2(A_4)_2B_{30}$, and (c) H-shaped terpolymer $(A_7)_2B_{30}(C_7)_2$.

The polymer molecules simulated in this work are illustrated in Figure 1. The H-shaped copolymers are of the type $(A_{N1})_2$-$B_{30}(A_{N2})_2$, where A represents the solvophilic beads and B the solvophobic ones. N_1 is the number of beads of each of the two equal length branches connected to one end of the solvophobic bridge B, and N_2 is the number of beads of each of the other two equal length branches, connected to the opposite end of the solvophobic bridge. The H-shaped terpolymers are of the type $(A_{N1})_2B_{30}(C_{N2})_2$, where A and C are the different solvophilic beads. For comparison purposes, miktoarm stars $(A_{N1})_2(A_{N2})_2$-B_{30} are also simulated. In all conducted simulations the solvophobic part B of polymers contains 30 beads.

The Brownian dynamics simulations were performed in a cubic box with periodic boundary conditions, using the open-source massive parallel simulator LAMMPS.[17,18] Previous works have proved the high efficiency of LAMMPS in the study of amphiphilic copolymers.[10,11] Different cutoff values in the Lennard-Jones potential were used[10,11] to describe the interactions between copolymer units with $\varepsilon_{ij} = \varepsilon$. The A−A and A−B interactions were considered repulsive and have cutoff radii $r_{cij} = 2^{1/6}\sigma$ while the B−B had an attractive potential with cutoff radius $r_{cij} = 2.5\sigma$. For the sake of simplicity, all beads A, B, and C were considered to have the same mass ($m = 1$) and diameter ($\sigma = 1$).

In this work system, sizes with 125 and 1000 polymeric chains were simulated. Amphiphiles were assumed to reside to the same micelle if the distance between any two nonbonded solvophobic beads B, belonging to different chains, was found within 1.5σ. This distance corresponds to the maximum extension of the FENE bonds.[10,11] The reduced temperature of the simulation T^* was set to $T^* = k_BT/\varepsilon = 1.8$. This choice of temperature allows the studied systems to have both micelles and free molecules.[11] If the temperature is very low, the studied system contains only aggregates and no free molecules; while if the temperature is very high, the studied system contains only free molecules and no aggregates. The system size was chosen so to ensure that the radius of gyration of the largest micelle to be at least the one-fourth of the box side length. For this particular reason we have used detailed exploratory runs with various simulation box sizes for low and high densities ensuring that every system studied shows identical aggregate size distributions. The use of the one-quarter of the simulation box side proved to be a sufficient condition to avoid interaction of chains and micelles with their images. No system size effects observed for all the calculated quantities reported on this paper.

The modeling of the ABC terpolymers was made in similar way. Different units were connected with FENE bonds. The FENE potential parameters ε and the temperature of the simulation ($T^* = 1.8$) were the same as in the case of ABA copolymers.

In order to create the chemical mismatch between the two solvophilic polymers A and C, weak attractions between the A−A and C−C units were introduced. The solvent conditions for A and C moieties start from theta solvent and increases progressively to good solvent. For the macroscopic states we studied, the solvent is considered to be bad for B units with A−C, A−B, and B−C heterointeractions being repulsive. The repulsions and the attractions between non-neighboring units were also described by Lennard-Jones potential with different cutoff distances. Repulsions had cutoff $r_{cij} = 2^{1/6}\sigma$ and well-depth $\varepsilon_{ij} = \varepsilon$. For the B−B, A−A, and C−C attractions, the cutoff radii is set to $r_{cij} = 2.5\sigma$ with $\varepsilon_{BB} = \varepsilon$, $\varepsilon_{AA} = \varepsilon_{CC} = 0.7\varepsilon$, 0.6ε, and 0.5ε corresponding to the different solvent conditions mentioned above. Brownian dynamics simulations, performed at the reduced temperature $T^* = 1.8$, on linear homopolymers containing 10, 20, 40, and 80 units with FENE bonds and Lennard-Jones interactions between them, gave a clear manifestation that theta solvent conditions correspond to $\varepsilon_{ij} = 0.7\varepsilon$. Under these conditions, the exponent 2ν of the radius of gyration R_g with respect to the total molecular weight ($R_g^2 \sim M_w^{2\nu}$) is equal to 1. When the value of ε_{AA} and ε_{CC} decreases, from 0.7ε to 0.5ε, the solvent quality within A and C moieties increases, reducing the chemical mismatch between them.[19] In all simulations, we set $\varepsilon = 1$.

In order to avoid bond crossing at the desired concentration, the ABA or the ABC polymer molecule was arranged on a lattice box. The energy of the chain was minimized and then the small system was replicated $N_{Polymer}$ times, equal to the number of polymer chains. We performed one million time steps with time step $\Delta t = 0.008\tau$ setting all cutoff radii equal to $r_{cij} = 2^{1/6}\sigma$ in order to eliminate any bias introduced from the initial conformation. The system then was allowed to equilibrate for five million steps. The simulation subsequently conducted for 15 million steps for the 125 polymer chains, and up to 50 or 60 million steps for larger systems with 1000 chains. The length of the simulation was evaluated by calculating the tracer autocorrelation function:

$$C(t) = \frac{\langle N(t_0+t)N(t_0)\rangle - \langle N(t_0)\rangle^2}{\langle N^2(t_0)\rangle - \langle N(t_0)\rangle^2} \quad (5)$$

where $N(t)$ is the number of molecules in the micelle, which a copolymer resides at time t. We took all copolymers as tracers, and every time step as a time origin t_0. The characteristic relaxation time t_c is defined as the required time for $C(t)$ to reach the value of e^{-1}. Each simulation was run at least $10t_c$ to have 10 independent conformations. The properties of interest were calculated as averages from 1500 and 5000 snapshots for the systems, with 125 and 1000 chain, respectively. For the large systems with 1000 polymer chains, every batch run was submitted on 14 processors and needed about 20 days in a parallel machine with Opteron 2.2 GHz CPU's to be completed.

3. Results and Discussion

3.1. H-Shaped Copolymers. *A. Critical Micelle Concentration.* In dilute solutions the copolymer chains under selective solvent conditions form aggregates. The reason is that the aggregates have much less entropy and thus reduce significantly the energy of the system: the free energy per chain in the aggregate is smaller than the respective energy of the free chain in the solution and this difference is the driving force of micellization in dilute solution of copolymers at constant temperature. In a particular concentration called critical micelle concentration (cmc) there is an abrupt increase in the fraction of chains involved in the formation of micelles. The onset of micellization is traditionally depicted by plotting the free (nonassociated) copolymer monomers concentration [F] as a function of the total copolymer monomers concentration [C]. The total copolymer concentration is defined as $[C] = N_w n/V$ where n is the number of copolymer molecules, N_w is the number of monomer beads per copolymer molecule, and V is the total volume of the simulation box. The maximum concentration [F] defines the cmc for that system.

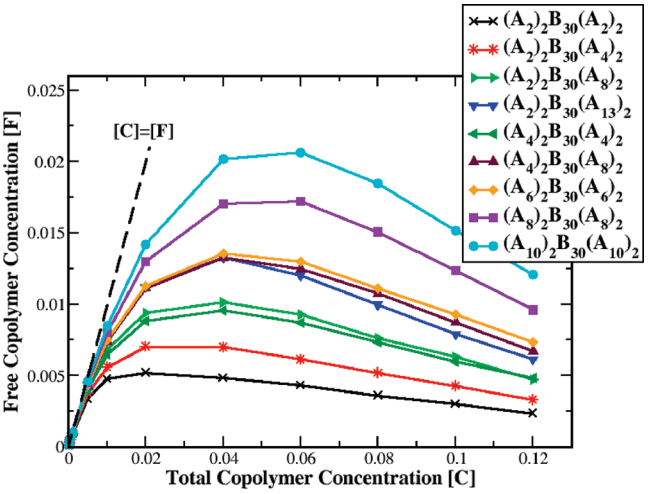

Figure 2. Concentration of free copolymers [F] versus the total copolymer concentration [C] for different H-shaped copolymers.

Figure 2 shows a plot of the free copolymer concentration against the total copolymer concentration for the simulated H-shaped copolymers $(A_{N1})_2B_{30}(A_{N2})_2$ with various branch lengths N_1, N_2. At higher concentrations, a decline in free copolymers concentration is observed. A similar trend is observed in simulations by other authors studying the cmc of copolymers having various architectures.[10,11] This decrease which is evident from experimental measurements[20] is not predicted by traditional theories[21] describing micelle formation, with the exception of the Leibler theory,[22] as noted by Adriani et al.[23]This theory suggests that excluded volume effects introduce a nonideal behavior at high copolymer concentrations [C] and that the accessible volume is considerably reduced driving more free chains to aggregate. The cmc values calculated from Figure 2 are given in Table 1.

The molecular theory for the formation of micelles can be used to describe qualitatively the trends of these values. According to the theory the mole fraction of micelles X_n with an aggregation number n is equal to

$$X_n = X_1 \exp(-g_{mic}/k_B T) \quad (6)$$

and inversely proportional to the cmc.[24] X_1 is the mole fraction of unimers and g_{mic} is the change in the Gibbs free energy associated with the transfer of n unimers from the solution to a micelle. This free energy for uncharged copolymers can be modeled as the sum of four different terms that takes into account all of the free energy changes that occur upon micelle formation $g_{mic} = g_{tr} + g_{int} + g_{pack} + g_{st}$. The first three terms are related to the solvophobic part of the copolymer, and the fourth is associated with the solvophilic counterpart. The free energy of transfer g_{tr} reflects the energy change associated with the transfer of the solvophobic block from the solution to micelles core. The interfacial free energy g_{int} takes into account the energy change upon formation of the interface between the core and the solution while g_{pack} involves the free energy change associated with constraining the end or ends of the solvophobic part to lie at the periphery of micelle core. The last term g_{st} accounts for the

Table 1. Cmc for Different H-Shaped and the Respective Miktoarm Star Copolymers

H-shaped copolymer	molecular weight	solvophobic content (%)	cmc_H	cmc_{Star}	r
$(A_2)_2B_{30}(A_2)_2$	38	78.9	0.0052	0.0016	3.75
$(A_2)_2B_{30}(A_4)_2$	42	71.4	0.007	0.0029	2.5
$(A_2)_2B_{30}(A_8)_2$	50	60	0.0102	0.0043	1.5
$(A_2)_2B_{30}(A_{13})_2$	60	50	0.0133	0.0071	1
$(A_4)_2B_{30}(A_4)_2$	46	65.2	0.0096	0.0039	1.88
$(A_4)_2B_{30}(A_8)_2$	54	55.6	0.0133	0.0063	1.25
$(A_6)_2B_{30}(A_6)_2$	54	60	0.0136	0.0066	1.25
$(A_8)_2B_{30}(A_8)_2$	62	55.6	0.0172	0.0088	0.94
$(A_{10})_2B_{30}(A_{10})_2$	70	48.4	0.0206	0.0113	0.75
$(A_{60})_2B_{30}(A_{60})_2$	270	11.1			0.125

contribution of steric interactions between the solvophilic units of the copolymers.

Table 1 indicates that for symmetric H copolymers $(A_{N1})_2B_{30}(A_{N2})_2$ (with equal length arms $N_1 = N_2$) the cmc values are proportional to the arm molecular weight. The larger the solvophilic arms become, the higher the steric penalties for transferring the large groups into the micelle. According to eq 6 g_{mic} increases and consequently cmc values increase. For asymmetric H-shaped copolymers $(A_{N1})_2B_{30}(A_{N2})_2$ with $N_1 = 4$ the increase of the molecular weight of the other two arms, $N_2 = 8, 16, 26$, increases the cmc for similar reasons. In addition to the molecular theory of micellization for linear AB copolymers, it was found that the cmc depends on the solvophobic−solvophilic balance.[10,11] The increase of the solvophobic/solvophilic molecular weight ratio r leads to the monotonic decrease of the cmc. In the case of H-shaped copolymers the dependence of the cmc on the ratio r is not always monotonic. The $(A_2)_2B_{30}(A_{13})_2$ copolymer with $r = 1$ has the same cmc value with the $(A_4)_2B_{30}(A_8)_2$ having $r = 1.25$. The reason is that the energetic penalty due to the steric interaction in $(A_2)_2B_{30}(A_{13})_2$ is higher because of the longer side arms ($N_2 = 13$). In H-shaped copolymers, $(A_4)_2B_{30}(A_8)_2$, $(A_6)_2B_{30}(A_6)_2$, with equal ratios $r = 1.25$ and almost similar branch lengths, higher cmc values exhibits the copolymer with the more symmetric arms. This is due to higher steric interactions between the arms. For comparison purposes we have also simulated four-arm miktoarm star copolymers of type $(A_{N1})_2(A_{N2})_2B_{30}$, where all branches were identical with the respective arms of the H-shaped copolymers $(A_{N1})_2B_{30}(A_{N2})_2$.

In Figure 3 we present the free chains concentration [F] against the total star copolymer concentration [C]. The resulting cmc_{star} values are summarized in Table 1. It can be observed that the cmc_{star} values are always lower compared to the respective values of the H-shaped counterparts. According to the molecular theory of micellization, the free energy change g_{pack} associated with constraining both ends of the solvophobic part B to lie in the periphery in H-shaped copolymers is higher than the respective free energy change associated with constraining the one end of the solvophobic part in miktoarm star copolymers. Thus, according to eq 6 cmc_{star} values are always lower than the cmc values of H-shaped copolymers. Figure 4 summarizes the cmc values of copolymers of both architectures having symmetric branches $N_1 = N_2$ against the ratio r. The fit of data illustrates that the cmc values have an exponential relationship with solvophobic/solvophilic molecular weight ratio r which could be represented by the following equations $cmc_H = 0.02858 \exp(-0.5372r)$, $cmc_{Star} = 0.02122 \exp(-0.8944r)$ for the H-shaped and star copolymer, respectively.

B. Micelle Size and Shape. The aggregation number, the radii of gyration of the solvophobic, solvophilic parts and of the whole aggregate as well as the resulting asphericities and acylindricities are useful tools for characterizing the micelles

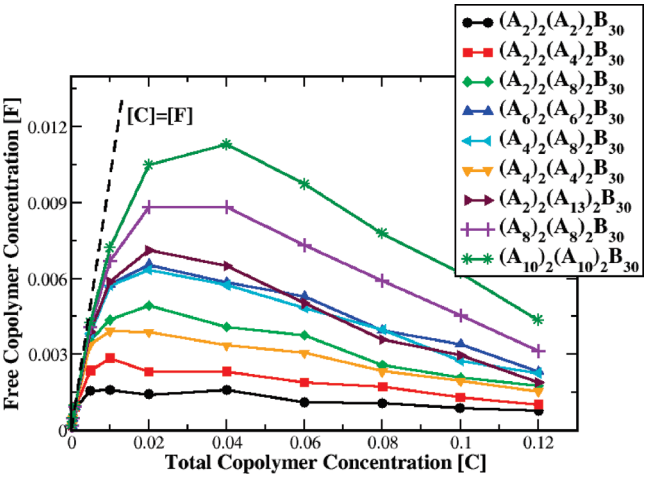

Figure 3. Concentration of free copolymers [F] vs the total copolymer concentration [C] for different mictoarm star copolymers.

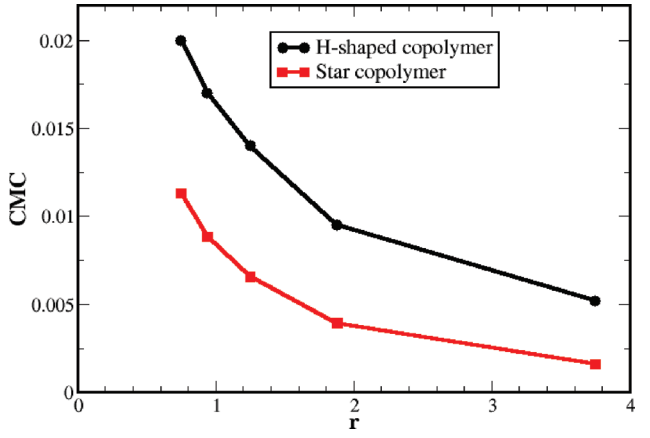

Figure 4. Cmc versus hydrophobic/hydrophilic ratio r for symmetric H-shaped and mictoarm star copolymers.

formed by amphiphilic copolymers. All these properties were calculated on the most concentrated system having [C] = 0.12 where most aggregates are formed. Figure 5 shows our results on the mass distribution of the aggregates for various H-shaped copolymers. The three regimes found in the experimental study of super-H copolymers[8] were also observed in our simulation results. The first regime containing the H-shaped copolymers is illustrated in Figure 5a. The mass distribution of the aggregates has a maximum value corresponding to the preferential aggregation number N_p of the formed micelles. One can observe that for symmetric H-shaped copolymers the most probable number of chains per aggregate decreases with the increase of the arms length due to the increase of the steric interactions in the micelle corona (Table 2).

For the symmetric H-shaped copolymers, the $(A_5)_2$-$B_{30}(A_5)_2$ copolymer containing a percentage of 60% solvophobic units is the lower limit of this regime. When the percentage of the solvophobic units is further decreased, a second regime is evident, where micelles with a wide aggregation number are formed (Figure 5b). The mass distribution of aggregates becomes a monotonic function with respect to the aggregation number and thus a mean aggregation number of micelles can be calculated. The symmetric H-shaped copolymer $(A_{60})_2B_{30}(A_{60})_2$ with 12% solvophobic units has a mean aggregation number equal to 1.47 and may be considered as the threshold of the third regime: the unimolecular micelles.

The first two regimes become wider in the case of asymmetric H-shaped copolymers since the steric effects between arms in the corona are weaker. Indeed, the $(A_2)_2B_{30}(A_{13})_2$ copolymer, that contains 50% solvophobic units, forms micelles with preferential aggregation number equal to 8, placing it in the first regime. For comparison purposes, we have calculated the mass distribution of aggregates of the respective $(A_{N1})_2(A_{N2})_2B_{30}$ star copolymers. Our results are listed in Figure 6. The mass distribution of the aggregates shows, in all cases, a bell-shaped form. The preferential aggregation numbers of the formed micelles, listed in Table 3, are about four times higher than the respective of H-shaped copolymers. The reason is the packing penalty associated

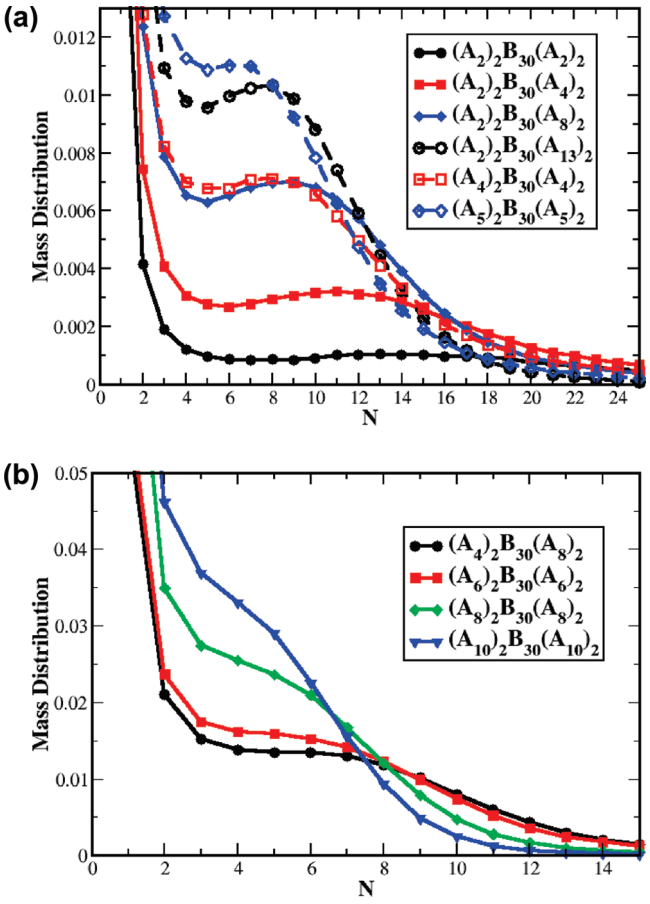

Figure 5. Mass distribution of the aggregates for various H-shaped copolymers: (a) aggregates following a bell-shaped distribution and (b) aggregates following a non-bell-shaped distribution.

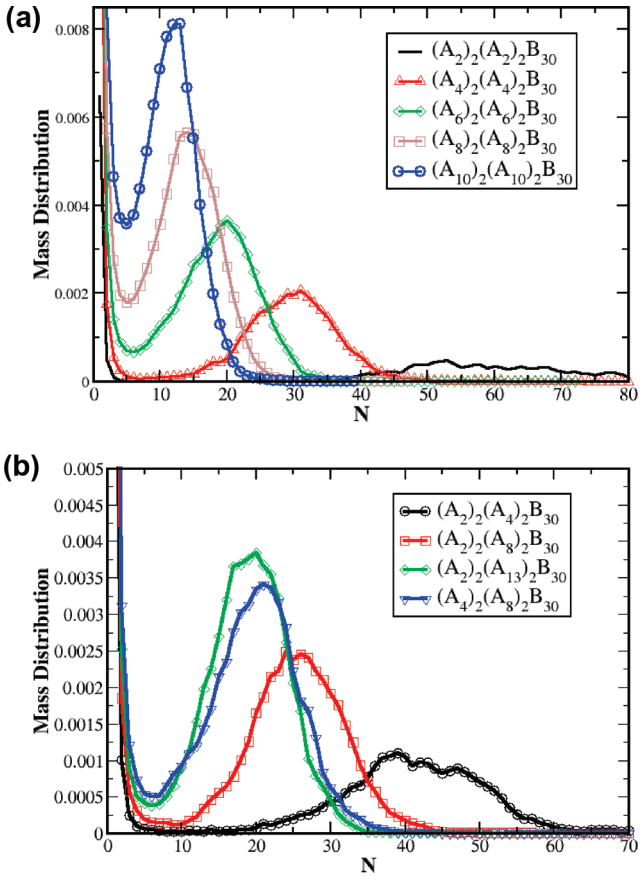

Figure 6. Mass distribution of the aggregates for various miktoarm star copolymers: (a) with equal length arms and (b) with asymmetric arms.

Table 2. Shape Characteristics of the Most Probable Aggregates Formed by H-Shaped Copolymers (Standard Deviation Is Inside the Parentheses)

H-shaped copolymer	N_P	$\langle R_g^2\rangle_{micelle}$	$\langle R_g^2\rangle_{core}$	$\langle R_g^2\rangle_{corona}$	H	R_c
$(A_2)_2B_{30}(A_2)_2$	13	32.1 (0.3)	27.5 (0.3)	49.2 (0.2)	0.54 (0.05)	6.76 (0.04)
$(A_2)_2B_{30}(A_4)_2$	11	32.9 (0.3)	25.7 (0.3)	50.7 (0.3)	0.86 (0.05)	6.54 (0.04)
$(A_2)_2B_{30}(A_8)_2$	9	36.2 (0.1)	22.9 (0.1)	55.8 (0.1)	1.59 (0.02)	6.17 (0.01)
$(A_2)_2B_{30}(A_{13})_2$	8	42.8 (0.1)	21.0 (0.1)	63.7 (0.2)	2.53 (0.02)	5.91 (0.01)
$(A_4)_2B_{30}(A_4)_2$	8	30.2 (0.1)	21.7 (0.1)	45.9 (0.1)	1.08 (0.02)	6.01 (0.01)
$(A_5)_2B_{30}(A_5)_2$	6	28.2 (0.1)	18.2 (0.1)	42.6 (0.1)	1.35 (0.02)	5.50 (0.02)
$(A_{60})_2B_{30}(A_{60})_2$	1	81.4 (0.4)	5.74 (0.02)	88.8 (0.5)	8.55 (0.03)	3.090 (0.005)

H-shaped copolymer	$\langle A_{sph}\rangle_{micelle}$	$\langle A_{sph}\rangle_{core}$	$\langle A_{sph}\rangle_{corona}$	$\langle A_{cyl}\rangle_{micelle}$	$\langle A_{cyl}\rangle_{core}$	$\langle A_{cyl}\rangle_{corona}$
$(A_2)_2B_{30}(A_2)_2$	0.303 (0.004)	0.344 (0.005)	0.235 (0.003)	0.097 (0.002)	0.105 (0.003)	0.093 (0.002)
$(A_2)_2B_{30}(A_4)_2$	0.292 (0.005)	0.351 (0.005)	0.242 (0.004)	0.096 (0.002)	0.106 (0.002)	0.099 (0.002)
$(A_2)_2B_{30}(A_8)_2$	0.270 (0.002)	0.354 (0.003)	0.250 (0.001)	0.100 (0.001)	0.108 (0.001)	0.111 (0.001)
$(A_2)_2B_{30}(A_{13})_2$	0.248 (0.002)	0.351 (0.003)	0.245 (0.001)	0.104 (0.001)	0.109 (0.001)	0.117 (0.001)
$(A_4)_2B_{30}(A_4)_2$	0.285 (0.003)	0.359 (0.003)	0.242 (0.002)	0.098 (0.001)	0.109 (0.001)	0.102 (0.001)
$(A_5)_2B_{30}(A_5)_2$	0.281 (0.002)	0.365 (0.003)	0.254 (0.001)	0.105 (0.001)	0.114 (0.001)	0.114 (0.001)
$(A_{60})_2B_{30}(A_{60})_2$	0.434 (0.001)	0.521 (0.002)	0.448 (0.001)	0.160 (0.001)	0.125 (0.001)	0.164 (0.001)

Table 3. Shape Characteristics of the Most Probable Aggregates Formed by Miktoarm Star Copolymers (Standard Deviation Is Inside the Parentheses)

star copolymer	N_P	$\langle R_g^2\rangle_{micelle}$	$\langle R_g^2\rangle_{core}$	$\langle R_g^2\rangle_{corona}$	H	R_c
$(A_2)_2(A_2)_2B_{30}$	53	63.5 (0.5)	52.0 (0.5)	106.7 (0.4)	0.98 (0.06)	9.30 (0.04)
$(A_2)_2(A_4)_2B_{30}$	39	60.4 (0.8)	44.3 (0.8)	100.3 (0.8)	1.4 (0.1)	8.59 (0.08)
$(A_2)_2(A_8)_2B_{30}$	24	57.1 (0.1)	33.3 (0.1)	92.5 (0.2)	2.30 (0.01)	7.44 (0.01)
$(A_2)_2(A_{13})_2B_{30}$	20	65.5 (0.2)	30.2 (0.2)	100.4 (0.2)	3.35 (0.02)	7.09 (0.02)
$(A_4)_2(A_4)_2B_{30}$	31	59.0(0.2)	39.4 (0.1)	95.5 (0.2)	1.81 (0.02)	8.10 (0.01)
$(A_4)_2(A_8)_2B_{30}$	21	58.3 (0.1)	32.2 (0.2)	90.5 (0.2)	2.53 (0.02)	7.32 (0.02)
$(A_6)_2(A_6)_2B_{30}$	20	56.6 (0.2)	31.7 (0.2)	87.4 (0.2)	2.44 (0.03)	7.26 (0.02)
$(A_8)_2(A_8)_2B_{30}$	14	55.1 (0.2)	26.4 (0.1)	81.6 (0.2)	2.95 (0.02)	6.63 (0.01)
$(A_{10})_2(A_{10})_2B_{30}$	13	60.6 (0.3)	26.0 (0.2)	86.2 (0.3)	3.46 (0.04)	6.58 (0.03)
star copolymer	$\langle A_{sph}\rangle_{micelle}$	$\langle A_{sph}\rangle_{core}$	$\langle A_{sph}\rangle_{corona}$	$\langle A_{cyl}\rangle_{micelle}$	$\langle A_{cyl}\rangle_{core}$	$\langle A_{cyl}\rangle_{corona}$
$(A_2)_2(A_2)_2B_{30}$	0.19 (0.01)	0.23 (0.01)	0.140 (0.008)	0.077 (0.005)	0.088 (0.005)	0.064 (0.003)
$(A_2)_2(A_4)_2B_{30}$	0.187 (0.006)	0.235 (0.007)	0.145 (0.004)	0.077 (0.001)	0.092 (0.002)	0.069 (0.001)
$(A_2)_2(A_8)_2B_{30}$	0.171 (0.003)	0.237 (0.004)	0.148 (0.002)	0.077 (0.001)	0.095 (0.001)	0.076 (0.001)
$(A_2)_2(A_{13})_2B_{30}$	0.159 (0.003)	0.245 (0.005)	0.145 (0.002)	0.076 (0.001)	0.097 (0.001)	0.076 (0.001)
$(A_4)_2(A_4)_2B_{30}$	0.184 (0.004)	0.242 (0.005)	0.150 (0.003)	0.076 (0.001)	0.092 (0.002)	0.071 (0.001)
$(A_4)_2(A_8)_2B_{30}$	0.178 (0.003)	0.252 (0.005)	0.157 (0.002)	0.079 (0.001)	0.096 (0.001)	0.078 (0.002)
$(A_6)_2(A_6)_2B_{30}$	0.183 (0.002)	0.255 (0.004)	0.162 (0.002)	0.080 (0.001)	0.098 (0.001)	0.079 (0.001)
$(A_8)_2(A_8)_2B_{30}$	0.189 (0.002)	0.271 (0.003)	0.176 (0.002)	0.087 (0.001)	0.101 (0.001)	0.088 (0.001)
$(A_{10})_2(A_{10})_2B_{30}$	0.186 (0.002)	0.280 (0.002)	0.175 (0.002)	0.086 (0.001)	0.103 (0.001)	0.087 (0.001)

Table 4. Cmc, Preferential Aggregation Number N_p, and Shape Anisotropy (κ^2) for Aggregates Formed by Linear−Dendritic Block, Linear Diblock, H-Shaped, and Miktoarm Star Copolymers (Standard Deviation Is Inside the Parentheses)

architecture	system	molecular weight	N_P	r	cmc	$\langle\kappa^2\rangle_{micelle}$	$\langle\kappa^2\rangle_{core}$
linear−dendritic diblock copolymer [11]	G2D1	37		4.3	0.0014		
	G3D1	45	38	2.0	0.0027	0.038 (0.003)	0.065 (0.006)
	G2D2	44	47	2.1	0.0024	0.038 (0.007)	0.07 (0.01)
	G4D1	61	19	0.97	0.0065	0.042 (0.008)	0.08 (0.02)
	G3D2	60	22	1.0	0.0052	0.036 (0.007)	0.08 (0.02)
	G2D4	58	27	1.1	0.0042	0.028 (0.008)	0.07 (0.02)
linear diblock copolymer[11]	G0D15	45	62	2.0	0.0021	0.029 (0.007)	0.06 (0.01)
	G0D31	61	41	0.97	0.0034	0.017 (0.005)	0.06 (0.02)
H-shaped copolymer	$(A_2)_2B_{30}(A_2)_2$	38	13	3.75	0.0052	0.118 (0.003)	0.149 (0.004)
	$(A_2)_2B_{30}(A_4)_2$	42	11	2.5	0.007	0.112 (0.004)	0.157 (0.004)
	$(A_4)_2B_{30}(A_4)_2$	46	8	1.88	0.0096	0.108 (0.002)	0.164 (0.003)
	$(A_2)_2B_{30}(A_{13})_2$	60	8	1.0	0.0133	0.083 (0.001)	0.156 (0.002)
	$(A_8)_2B_{30}(A_8)_2$	62		0.94	0.0172		
star copolymer	$(A_2)_2(A_2)_2B_{30}$	38	53	3.75	0.0016	0.050 (0.006)	0.068 (0.008)
	$(A_2)_2(A_4)_2B_{30}$	42	39	2.5	0.0029	0.047 (0.003)	0.073 (0.005)
	$(A_4)_2(A_4)_2B_{30}$	46	31	1.88	0.0039	0.046 (0.002)	0.076 (0.003)
	$(A_2)_2(A_{13})_2B_{30}$	60	20	1.0	0.0071	0.035 (0.001)	0.080 (0.003)
	$(A_8)_2(A_8)_2B_{30}$	62	14	0.94	0.0088	0.049 (0.001)	0.096 (0.002)

with the solvophobic part in the core of the micelles in the case of H-shaped copolymers.

The shape of the micelles is described by calculating the asphericity A_{sph} and the acylindricity A_{cyl} using the principal components of the mean square radius of gyration tensor[25] S_x^2, S_y^2, S_z^2

$$A_{sph} = \left[\langle S_x^2\rangle - \frac{1}{2}\left(\langle S_y^2\rangle + \langle S_z^2\rangle\right)\right]/\langle S^2\rangle \quad (7)$$

$$A_{cyl} = \left(\langle S_y^2\rangle - \langle S_z^2\rangle\right)/\langle S^2\rangle \quad (8)$$

where $S_x^2 > S_y^2 > S_z^2$. For a rigid rod, the acylindricity is zero and the asphericity is near one. For spheres, both acylindricity and asphericity are close to zero. From the scaling point of view three types of micelles are defined on the basis of the relative size of their core radius R_c with respect to the corona thickness H. A micelle has a star like shape when $H \gg R_c$. The micelle has a crew-cut shape when the radius of the core is much larger of the thickness of the corona ($R_c \gg H$), while in other cases the micelle has an intermediate shape.[8] The radius of the core R_c can be calculated from its mean square radius of gyration by the following relation $R_{gcore}^2 = (3/5)R_c^2$. Similarly the thickness of the corona H can be obtained as the difference of the radii of the whole micelle and the core ($H = R_{mic} - R_c$). Our results on the shape of the most probable micelles for the H-shaped and the respective star copolymers are summarized in Tables 2 and 3. We can see that the monomolecular micelle formed by the $(A_{60})_2B_{30}(A_{60})_2$ H-shaped copolymer is the less spherical. The asphericity of the other micelles decreases as the length of the side arms increases, with the most spherical micelle formed by the asymmetric $(A_2)_2B_{30}(A_{13})_2$ copolymer having the longest side arms. The core of the micelles of the symmetric H copolymers becomes less spherical as the length of the side arms increases. Except for the monomolecular micelle of the $(A_{60})_2B_{30}(A_{60})_2$ copolymer, which is clearly starlike, all the other micelles can be characterized as crew-cut. The respective micelles formed by the star copolymers are clearly more spherical as indicated from the asphericity and acylindricity values of Table 3. The micelles obtained from $(A_{10})_2B_{30}(A_{10})_2$ stars can be characterized as intermediate while the others have a crew-cut shape.

C. Comparison with Other Simulation Results. Some of our results on H-shaped copolymers can be directly compared with respective simulation findings of ref 11 concerning the micellization properties of linear diblock and linear−dendritic diblock copolymers. Linear and linear−dendritic

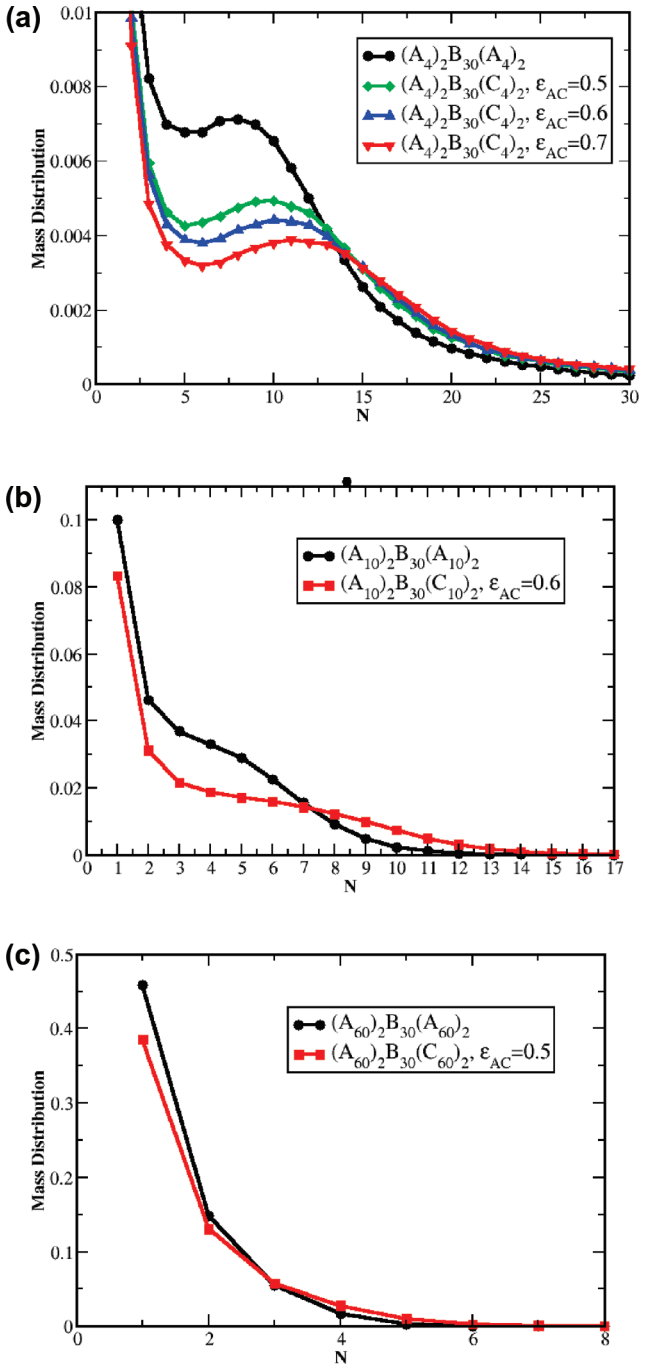

Figure 7. Mass distribution of the aggregates for H-shaped terpolymers (a) $(A_8)_2B_{30}(C_8)_2$ for different Lennard-Jones interactions parameters (ε_{AC}), (b) $(A_{20})_2B_{30}(C_{20})_2$, and (c) $(A_{60})_2B_{30}(C_{60})_2$. In all cases, the respective H-shaped copolymers are included.

copolymers contain 30 solvophobic units and their micellalization behavior was studied at the reduced temperature $T^* = 1.8$, also used in our simulations. The preferential aggregation number, the cmc and the shape anisotropy[27,28] κ^2 (denoted as δ in ref 11) are listed in Table 4. Linear diblock copolymers G0D15 and G0D31 contain solvophilic blocks with 15 and 31 units, respectively. The dendritic blocks are considered solvophilic. Dendritic moieties are of second (G2), third (G3), and fourth (G4) generation with branch length equal to one (D1), two (D2) or four (D4) beads.

It can be observed that for copolymers with different architectures but similar molecular weights the cmc values follow the inequality $\text{cmc}_{\text{linear}} < \text{cmc}_{\text{linear-dendritic}} < \text{cmc}_{\text{star}} < \text{cmc}_{\text{H-shaped}}$. This reflects the different steric interactions between solvophilic units in the corona and the change in free energy, associated with constraining the end or ends of the solvophobic part to lie on the periphery of micelle core. The preferential aggregation number N_p follows the opposite inequality $N_{p\ linear} > N_{p\ linear-dendritic} > N_{p\ star} > N_{p\ H\text{-}shaped}$. The micelle core shape anisotropy of linear, linear−dendritic and star copolymers has almost identical values while the respective quantity for the H-shaped copolymers is higher, indicating a less spherical topology. As far as the total micelle shape anisotropy is concerned one can observe that the most spherical micelles are formed by linear diblock copolymers. Linear−dendritic diblock, star, and H-shaped copolymers show increasing deviation from the spherical topology.

3.2. H-Shaped Terpolymers. Three different H-shaped terpolymers with equal length arms were simulated. Namely, the $(A_4)_2B_{30}(C_4)_2$, $(A_{10})_2B_{30}(C_{10})_2$, and $(A_{60})_2B_{30}(C_{60})_2$. Each one of the homologous H-shaped copolymers belongs to a different regime according to the mass distribution of the formed micelles. The $(A_{60})_2B_{30}(A_{60})_2$ forms monomolecular micelles. The $(A_{10})_2B_{30}(A_{10})_2$ forms micelles with vastly ranging aggregation numbers, while $(A_4)_2B_{30}(A_4)_2$ drives the formation of micelles containing 8 chains. To study the effect of the chemical mismatch between the solvophilic units A and C we have used three different values of A−A and C−C interaction parameters ($\varepsilon_{AA} = \varepsilon_{CC} = 0.7\varepsilon$, 0.6ε, and 0.5ε with $\varepsilon = 1$) in the Lennard-Jones potential. The higher the ε_{AA}, ε_{CC} values the higher the mismatch between A and C units. Our simulation results for the mass distribution of the formed micelles at the reduced temperature $T^* = 1.8$ are shown in Figure 7. It can be observed (Figure 7a, Table 5) that the $(A_4)_2B_{30}(C_4)_2$ terpolymers form micelles having greater aggregation number than the respective copolymer. The decrease of the mismatch between the A, C units leads to the decrease of the aggregation number. This trend is the opposite of the assumption and reasoning of the experimental group who studied super H-shaped copolymers[8] and H-shaped terpolymers.[9] In our opinion, the reason for this discrepancy are the different thermodynamics conditions, between copolymers and terpolymers, used in their micellization study.

Table 5. Shape Characteristics of the Most Probable Aggregates Formed by H-Shaped Terpolymers (Standard Deviation Is Inside the Parentheses)

H-shaped terpolymer	N_P	ε_{AC}	$\langle R_g^2\rangle_{mic}$	$\langle R_g^2\rangle_{core}$	$\langle R_g^2\rangle_{corona}$	H	R_c
$(A_4)_2B_{30}(C_4)_2$	10	0.5	33.1 (0.2)	24.1 (0.2)	49.8 (0.1)	1.09 (0.03)	6.33 (0.03)
$(A_4)_2B_{30}(C_4)_2$	10	0.6	32.7 (0.2)	23.7 (0.2)	49.3 (0.2)	1.10 (0.03)	6.28 (0.03)
$(A_4)_2B_{30}(C_4)_2$	11	0.7	34.1 (0.2)	24.9 (0.3)	51.3 (0.3)	1.10 (0.05)	6.44 (0.04)
$(A_{60})_2B_{30}(C_{60})_2$	2	0.5	88.3 (0.4)	9.4 (0.8)	97.3 (0.5)	8.2 (0.2)	4.0 (0.2)

H-shaped terpolymer	$\langle A_{sph}\rangle_{micelle}$	$\langle A_{sph}\rangle_{core}$	$\langle A_{sph}\rangle_{corona}$	$\langle A_{cyl}\rangle_{micelle}$	$\langle A_{cyl}\rangle_{core}$	$\langle A_{cyl}\rangle_{corona}$
$(A_4)_2B_{30}(C_4)_2$	0.278 (0.003)	0.352 (0.003)	0.230 (0.002)	0.093(0.001)	0.106 (0.001)	0.095 (0.001)
$(A_4)_2B_{30}(C_4)_2$	0.272 (0.003)	0.345 (0.003)	0.226 (0.003)	0.093(0.001)	0.106 (0.001)	0.095 (0.001)
$(A_4)_2B_{30}(C_4)_2$	0.269 (0.005)	0.344 (0.005)	0.221 (0.004)	0.091 (0.001)	0.104 (0.001)	0.092 (0.001)
$(A_{60})_2B_{30}(C_{60})_2$	0.332 (0.003)	0.436 (0.003)	0.328 (0.003)	0.146 (0.002)	0.138 (0.001)	0.149 (0.002)

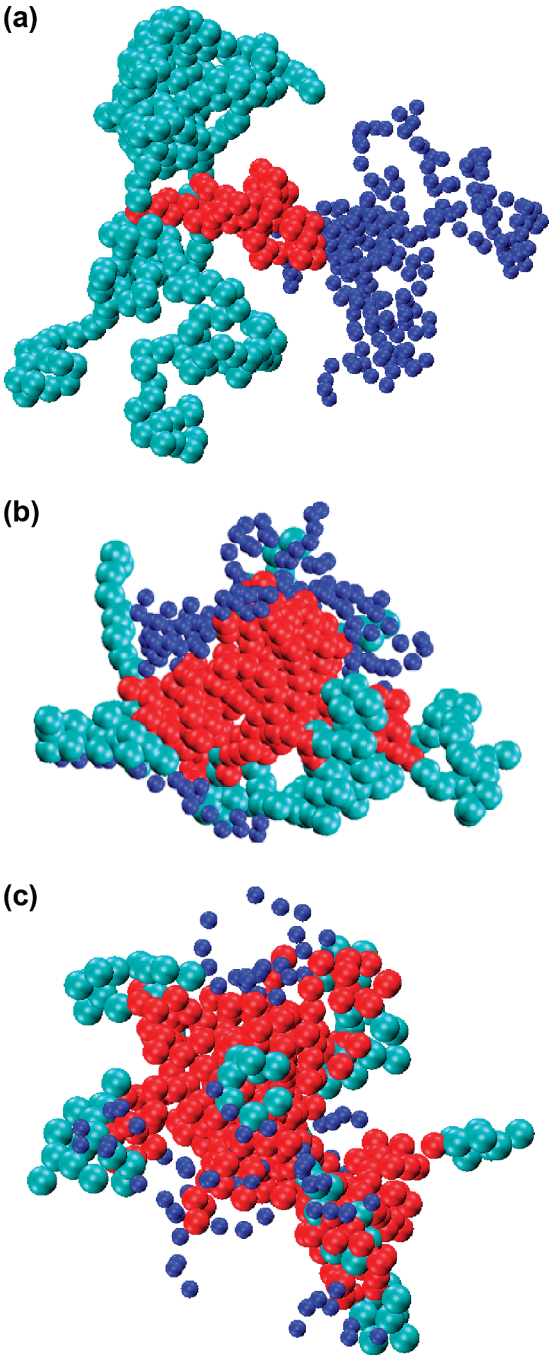

Figure 8. Snapshots of micelles formed by (a) $(A_{60})_2B_{30}(C_{60})_2$ with aggregation number $N_P = 2$ and $\varepsilon_{AC} = 0.5$, (b) $(A_{20})_2B_{30}(C_{20})_2$ with $N_P = 7$ and $\varepsilon_{AC} = 0.6$, and (c) $(A_4)_2B_{30}(C_4)_2$ with $N_P = 11$ and $\varepsilon_{AC} = 0.7$.

The *n*-decane is a very strong precipitant for the polystyrene in comparison with the MEK precipitant for the polybutadiene. Our results exactly correspond to the same molecular weights and thermodynamic conditions for the solvophobic polymer moieties ($T^* = 1.8$).

Similar are the results for the $(A_{10})_2B_{30}(C_{10})_2$, presented in Figure 7b. The free chains and micelles with small aggregation number are less than the respective of the H-shaped copolymer while the micelles having greater aggregation number are clearly more. In the case of $(A_{60})_2B_{30}(C_{60})_2$ terpolymer (Figure 7c) the mean aggregation number is 1.63 compared to the 1.47 of the respective copolymer. Figure 8 illustrates snapshots of aggregated terpolymers $(A_{60})_2B_{30}(C_{60})_2$, $(A_{10})_2B_{30}(C_{10})_2$, and $(A_4)_2B_{30}(A_4)_2$ with aggregation numbers 2, 7, and 11 respectively. One can observe that the micelles of the $(A_{60})_2B_{30}(C_{60})_2$ terpolymers are Janus-like with the segregated A and C blocks surrounding the insoluble B block. This picture is in agreement with the Scheme 6 of ref 9. The micelles of the $(A_{10})_2B_{30}(C_{10})_2$ with small aggregation numbers are also Janus like. Micelles having large aggregation numbers present Janus-like faces incorporating patches consisting of the opposite type units (Figure 8b). The number of patches is increased in the micelles formed by terpolymers with short arms driving the formation of aggregates with a multicompartment corona (Figure 8c). Table 5 shows the characteristic shape and size of the most probable aggregate for the three terpolymers studied.

4. Conclusions

The micellization behavior of H-shaped copolymers and terpolymers are studied with Brownian dynamics simulations at the reduce temperature $T^* = 1.8$. Our results come to promote and refine the experimental findings of Hadjichristidis group[8,9] and can be summarized as follows: symmetric H-shaped copolymers with a large weight fraction of solvophobic units ($\geq$60%) form micelles with a preferential aggregation number. Those with smaller ($\geq$10%) solvophobic content form micelles with varying aggregation number while the rest H-shaped copolymers with solvophobic units fraction ($\leq$10%) do not aggregate at this temperature. The asymmetric H-shaped copolymers form micelles with preferential aggregation number at smaller ($\geq$50%) solvophobic content and do not aggregate at solvophobic fraction ($\ll$10%). These regimes are in qualitative agreement with experiment. We found that the H-shaped terpolymers form micelles with higher aggregation numbers compared to the respective H-shaped copolymers. When the chemical mismatch between solvophilic A and C units increases the symmetric H-shaped terpolymers with long arms form Janus like micelles. Those with small arm length aggregate to micelles with a multicompartment corona.

Acknowledgment. We would like to thank Professors Monica Lamm and Dapeng Cao for their help on using LAMMPS simulation package. The research Center for Scientific Simulations (RCSS) of the University of Ioannina is gratefully acknowledged for providing the computer resources used in this work.

References and Notes

(1) Hadjichristidis, N.; Pispas, S.; Floudas, G. Block Copolymers, Synthetic Strategies. In *Physical Properties and Applications*; Wiley-Interscience: Hoboken, NJ, 2003.
(2) Riess, G. *Prog. Polym. Sci.* **2003**, *28*, 1107–1170.
(3) Poulos, Y.; Pispas, S.; Hadjichristidis, N. H. *Macromolecules* **1998**, *31*, 4177–4181.
(4) Mountrichas, G.; Mpiri, M.; Pispas, S. *Macromolecules* **2005**, *38*, 940–947.
(5) Nguyen, P.; Hammond, P. *Langmuir* **2006**, *22*, 7825–7832.
(6) Djalali, R.; Hugenberg, N.; Fischer, K.; Schmidt, M. *Macromol. Rapid Commun.* **1999**, *20*, 444–449.
(7) Pispas, S.; Hadjichristidis, N.; Mays, J. *Macromolecules* **1996**, *29*, 7378–7385.
(8) Iatrou, H.; Willner, L.; Hadjichristidis, N.; Halperin, A.; Richter, D. *Macromolecules* **1996**, *29*, 581–591.
(9) Christodoulou, S.; Driva, P.; Iatrou, H.; Hadjichristidis, N. *Macromolecules* **2008**, *41*, 2607–2615.
(10) Cheng, L.; Cao, D. *Langmuir* **2009**, *25*, 2749–2756.
(11) Suek, N.; Lamm, M. *Langmuir* **2008**, *24*, 3030–3036.
(12) Kim, K.; Kim, S.; Huh, J.; Jo, W. *J. Chem. Phys.* **2003**, *119*, 5705–5710.
(13) Gangwal, S.; Cayre, O.; Velev, O. *Langmuir* **2008**, *24*, 13312–13320.
(14) Kremer, K.; Grest, G. *J. Chem. Phys.* **1990**, *92*, 5057–5086.
(15) Lin, S.; Numasawa, N.; Nose, T.; Lin, J. *Macromolecules* **2007**, *40*, 1684–1692.

(16) Shen, T.; Wong, C.; McCammon, A. *Biopolymers* **2003**, *70*, 252–259.
(17) http://lammps.sandia.gov
(18) Plimpton, S. *J. Comput. Phys.* **1995**, *117*, 1–19.
(19) Joanny, J. F.; Leibler, L.; Ball, R. *J. Chem. Phys.* **1984**, *81*, 4640–4656.
(20) Johnson, I.; Olofsson, G.; Jonsson, B. *J. Chem. Soc., Faraday Trans.1* **1987**, *83*, 3331–3344.
(21) Goldstein, R. *J. Chem. Phys.* **1986**, *84*, 3367–3378.
(22) Leibler, L.; Orland, H.; Wheeler, J. *J. Chem. Phys.* **1983**, *79*, 3550–3557.
(23) Adriani, P.; Wang, Y.; Mattice, W. *J. Chem. Phys.* **1994**, *100*, 7718–7721.
(24) Nagarajan, R. *Langmuir* **1985**, *1*, 331–341.
(25) Gergidis, L.; Moultos, O.; Georgiadis, C.; Kosmas, M.; Vlahos, C. *Polymer* **2009**, *50*, 328–335.
(26) Murat, M.; Grest, G. *Macromolecules* **1996**, *29*, 1278–1285.
(27) Zacharopoulos, N.; Economou, I. *Macromolecules* **2002**, *35*, 1814–1821.
(28) Theodorou, D. N.; Suter, U. W. *Macromolecules* **1985**, *18*, 1206–1214.